The use of Calibrated Liquid Crystals for Measuring Shear Stress at Mach 4

PETER J DISIMILE[1], NORMAN TOY[2], AKSHAY SHERIKAR[2]
[1]Department of Aerospace Engineering and Engineering Mechanics,
University of Cincinnati,
Cincinnati, Ohio 45221,
USA

[2]Engineering and Scientific Innovations, Inc.,
Fairfield, Ohio 45014,
USA

Abstract: - A mechanical calibration rig has been used to calibrate shear stress-sensitive liquid crystals and to use this calibration for the measurement of the shear stress around a protuberance on the floor of a Mach 4 wind tunnel. The protuberance is of an equilateral triangular planform with a side dimension of 5.5mm, and with the apex pointing upstream. Two heights of protuberances were investigated, one being 1.5mm in height, and the other 3.0mm in height. The resulting bow shock and the trailing wake have been identified and the result shows how the magnitude of the shear stress diminishes immediately behind the bow shock. Furthermore, it is also shown how the shear stress increases on either side of the shock structure, as well as the rapid changes in the shear stress magnitude within the wake.

Key-Words: - Shear Stress, Liquid Crystals, Mach 4, Calibration, 3-dimensional Protuberance, Bow shock.

Received: July 14, 2024. Revised: November 3, 2024. Accepted: December 5, 2024. Published: January 30, 2025.

1 Introduction

The ability to provide a non-intrusive measurement system for acquiring surface shear stress in high-velocity flow fields is of paramount importance in the determination of skin friction forces acting on air-borne platforms. Furthermore, the capability for measuring the full-field boundary layer skin friction in supersonic and hypersonic flow cannot be overstated. For both supersonic and hypersonic flows, such measurements for determining the skin friction distribution (surface shear stress) as a non-intrusive technique are of importance, particularly for separating and reattaching flows on planar and curved surfaces. One such technique that has been examined over many years is that of using optically active Liquid Crystals of both the Chiral-Nematic and Cholesteric types.

Primarily, Liquid Crystals (LC) may be used both quantitatively and qualitatively on a surface in aerodynamic testing because of their optical activity, [1]. These types of crystals have a molecular structure between that of a crystalline solid and an isotropic liquid such that they possess the aero-mechanical properties of liquids but the optical properties of crystalline solids. This is advantageous in aerodynamic, aerothermal, and heat transfer measurements as compared to point measurement techniques since full-field or global distribution of the investigated parameter may be achieved.

Temperature-sensitive LC is rendered insensitive to shear by microencapsulation i.e. small

droplets of the LC are contained in transparent spheres made from a suitable polymer, whereas ‘neat’ unencapsulated LC are sensitive to external applied shear stress and may be made insensitive to a particular temperature range by mixing with other chemicals/substances, [2].

The ability of LC to reflect incident white light in a highly directional manner makes them ideal as a non-intrusive global wall shear stress measurement technique, [3], [4]. Digitized color images may be converted into a shear stress vector field once calibrated, with high spatial and temporal resolution with color information usually stored as separate red, green, and blue (R, G, and B) components as represented by the color triangle, Figure 1.

However, color (and hence Shear Stress) determined directly from these components is difficult since the values also contain information about light intensity, which may not be as uniform as required.

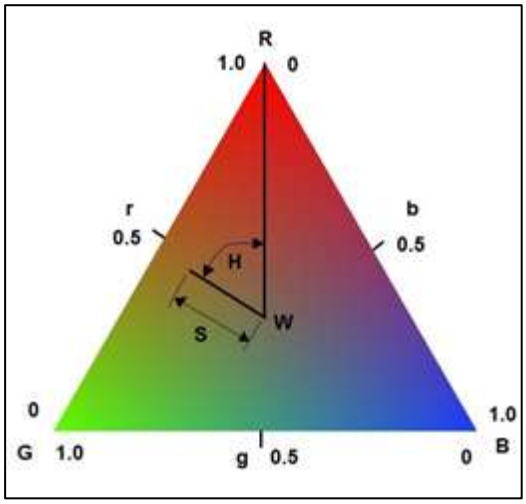

Fig. 1: A typical color triangle showing the relationship between R, G, B and H, S, I

A method commonly employed to overcome this difficulty is to transform the R, G, and B coordinates into Hue, Saturation, and Intensity (H, S, I), [5], for example:

$$H = 90 - \tan^{-1}\left(\frac{F1}{\sqrt{3}}\right) + F2 \qquad (1)$$

where

$$F1 = \frac{2R - G - B}{G - B}$$

and

$$F2 = \begin{cases} 0 & G \geq B \\ 180 & G < B \end{cases}$$

with

$$I = \frac{R+G+B}{3} \text{ and } S = 1 - \frac{\min(R,G,B)}{I}$$

Here, the color information is solely integrated within the value of H in which the results are given in degrees, illustrating that hue is an angular representation of color, with the primary colors R, G, and B taking hue values of 0, 120, and 240 degrees, respectively. It should be noted that there are a number of versions of these color transformations and care must be exercised in the application of them, [6].

One of the challenges of using LC in the measurement of the magnitude and direction of the shear stress vector is its calibration, since color play obtained from LC is highly sensitive to and depends upon the direction of the shear vector, lighting, and viewing angles, and thickness of the LC coating. Typically, there are two methods of calibration; (i) use of mechanical rigs for calibration [7], [8] and (ii) aerodynamic calibration [9], [10], [11], [12], [13]; a far more difficult and less effective technique, [14]. Furthermore, the physical properties of LC also play an important role and the choice of LC must match the testing program in order that they remain optically active, have high sensitivity to shear stress and low sensitivity to temperature, and have a viscosity that precludes excessive flow that may cause oil-flow patterns reminiscent of flow visualization, [15].

Although two types of mechanical calibration rigs were considered, a planar rig, and a rotational rig, initial designs, and experiments showed that even though the rotational rig would be more complex, it would provide the accuracy and future developmental capabilities that were required to calibrate the LC for thickness, shear stress, lighting, and viewing angles. Consequently, an apparatus was designed and assembled such that LC could be placed on an annular ring of known area and sandwiched between two circular plates with a fixed, but adjustable, separation distance. This distance could be varied between 40-150 microns, with the black anodized plate fixed to a rotational mechanism and the upper clear plate free, but restrained from rotation by a force balance, Figure 2.

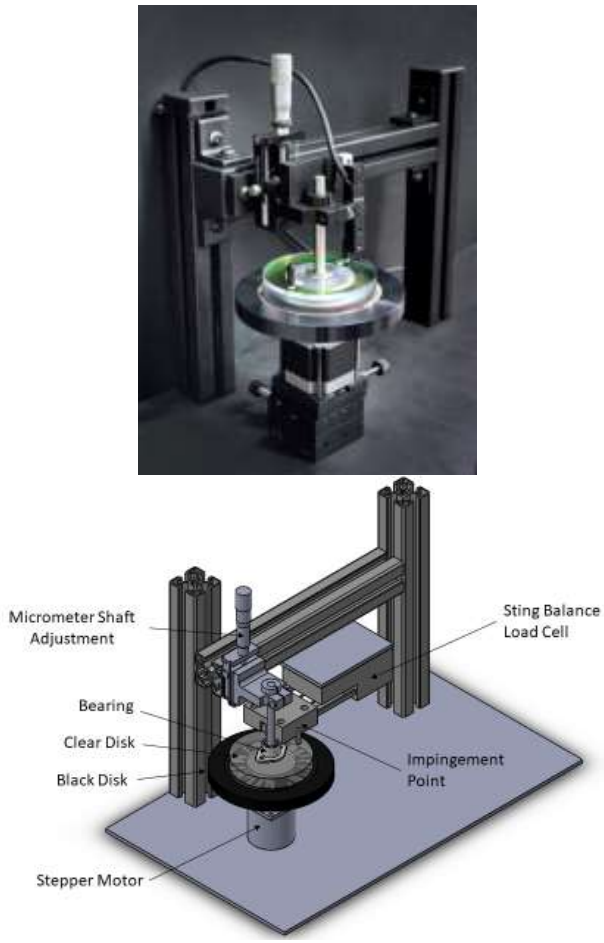

Fig. 2: Initial Design of Calibration Rig and Assembled Version

Furthermore, the lower black anodized disk has two 2.5 mm radius concentric gullies machined at 27.5 mm and 52.5 mm, and the clear upper disk has an annulus, with an inner radius of 30mm and an outer radius of 50mm, of the same area as that of the black disk. This design ensures that LC may be applied to the annular surface that is 20mm wide with any excess LC allowed to escape into the concentric gullies during the calibration procedure.

An example of how an LC sample is calibrated is as follows but does not include the details of illuminating and visualizing the annular surface:

- the upper clear disk is lowered onto the lower black anodized disk using the vertical positioning micrometer and adjusted to zero.
- The clear disk is then raised, allowing a thin layer of LC to be applied evenly to the black anodized aluminum disk.
- The micrometer is then used to lower the clear disk onto the LC at a pre-determined gap (20 – 150 μm), thereby setting the thickness of the applied liquid crystal layer.
- A stepper motor is used to rotate the lower black disk at a given rotational speed (ω) with the upper disk restrained by an impinging pin, set to the radial mid position of the annulus (40 mm), and pressing on a load cell.

The shear stress (τ) the liquid crystal is undergoing is determined by Newton's Law of Viscosity:

$$\tau = \mu \frac{du}{dy} = F/A \qquad (2)$$

where *dy* is the distance between the two disks set by the micrometer, and *du* is the rotational speed at a given radius, *F* is the restraining force and *A* is the area of the annulus. The dynamic viscosity μ of the LC is given by the Manufacturer's Specification.

As previously reported, the importance of illumination angle and viewing angle cannot be underestimated especially for measurements taken on curved surfaces where both illumination and viewing angles may have strong effects on the recorded hue value, [15]. However, for a planar surface, such as for the above calibration technique, a viewing angle of 'normal' to the area of interest, and an illumination of 45^0 to the normal, provides a strong reflectance signal from the LC and thereby a strong color change with surface shear stress. This is characterized in the following Figure 3 where the change in color (hue) is plotted against the applied shear stress in the calibration rig. Here, two different thicknesses of LC of BCN165 (having a relative viscosity of approximately 1000 CPS as provided by LCRHallcrest) have been applied (22 μm and 112 μm) and the results are very similar over the shear stress range of 40 – 1000 Pa, with a small difference of about 6% over the range of 40 – 300 Pa. A calibration curve fit to both sets of data is provided by a 5^{th} order polynomial, with an R^2 value of 0.993 thereby showing a good correlation.

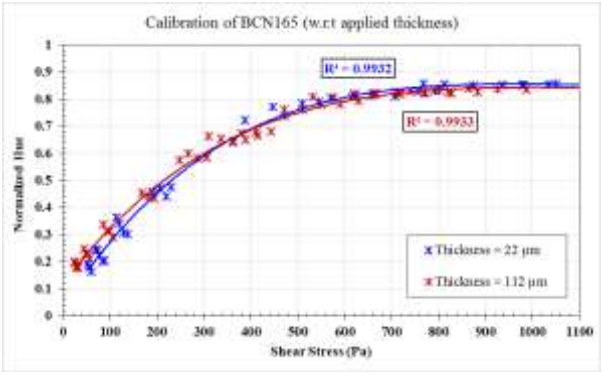

Fig. 3: Typical Calibration curves for BCN165

2 Experimental Facility

A Mach 4 wind tunnel was purposely designed and constructed for this investigation. Compressed air, held in a 2,800-litre tank was suddenly released through a fast-acting regulator valve and dryers to a large plenum chamber. The air was then discharged through a 2-D subsonic converging nozzle, mounted within the chamber, and a sonic nozzle of 1.422cm x 15.24cm dimensions, through a supersonic diverging section, designed by the Method of Characteristics that allowed for a flow of Mach 4 in the test section. Downstream of the test section, a supersonic diffuser was designed to reduce the required start-up time of the pressure ratio that ensures sonic conditions at the throat, Figure 4.

Fig. 4: Diagram of Mach 4 wind tunnel

The test section begins at the outlet of the supersonic nozzle and has dimensions of 15.24cm x 15.24cm in cross-section and 0.9m in length. Liquid Crystal tests were carried out at a location on the floor of the test section some 685 mm from the nozzle exit plane, with a Reynolds number of 2.32 x 10^7. Viewing of the LC and its illumination could be arranged through the window at the top of the test

section where a 45 degree -unobstructed line of sight could be applied, Figure 5. An area of approximately 40 mm x 60 mm in length immediately below the center of the viewing window was chosen for the location of the protuberances and used for the LC analysis.

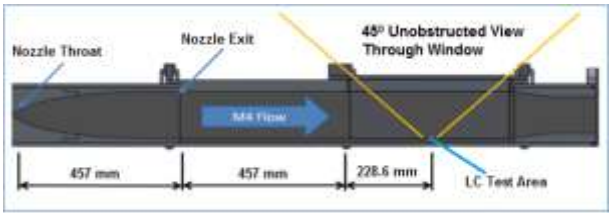

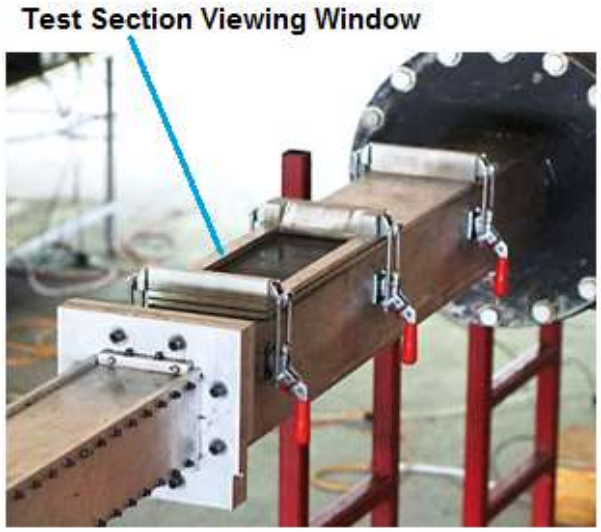

Fig. 5: Location of LC Measurement area in the Test Section and view of Window

3 Calibrated Liquid Crystal

The measuring site on the bottom of the tunnel was carefully prepared with Petroleum Ether and allowed to dry. A mixture of liquid crystal BCN165 and Petroleum Ether was then sprayed onto the surface and a Chronos 2.1 high-speed color video camera was installed above the window, perpendicular to the test area. Illumination of the test area was arranged with a Halogen spot lamp at an angle of 45^0 to the vertical, in the direction of shear.

Once the wind tunnel is operated, the air is immediately drawn through the plenum chamber and supersonic nozzle to the test section, and takes approximately 3 seconds before the shock passes through. Once the shock has passed, the tunnel is operating at its design speed of Mach 4 and this continues for a further 5 seconds, after which the air in the storage tank is exhausted.

Figure 6 shows the uniformity of the shear stress distribution at the test location just before the shock passes (t = 3 s), and again at the 5-second mark (t = 8 s), with Hue values, calculated using Equation 1, being 0.031 and 0.32 respectively. Using the calibration from Figure 3, the shear stress was determined to be 110 Pa over the area with a variation of less than 3 Pa.

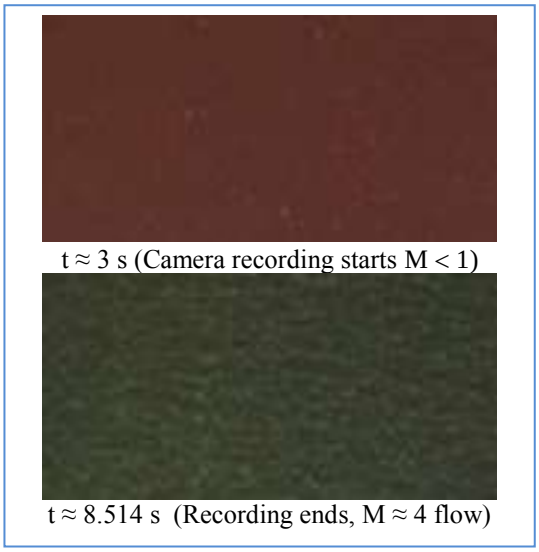

Fig. 6: Uniformity of LC at the test domain

By measuring the global shear stress created by 3-D protrusions, our increased understanding of skin friction may assist the CFD/simulation community, thereby improving future designs.

4 Shear Stress Distribution Caused by Wedge Shaped Protrusion

At high speed, where shock waves and turbulent boundary layers interact, small protuberances may give rise to changes in the local shear stress that can affect the drag forces of the platform. Unfortunately, little is known about the development and distribution of local shear stresses created by such small protuberances.

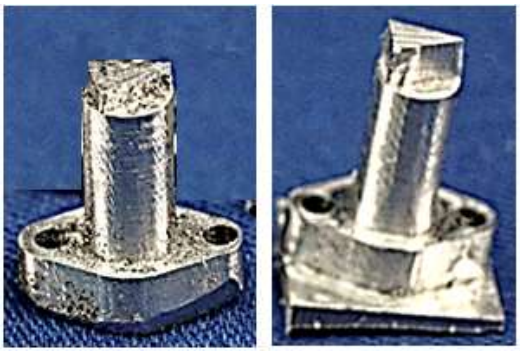

1.5 mm deep wedge **3.0 mm deep wedge**

Fig. 7: Two equilateral triangular wedge-shaped protrusions fabricated on circular plug

As an example, a small equilateral triangular wedge-shaped protrusion was fabricated on the surface of a 6.35 mm diameter plug that can be inserted into the bottom of the test section, with the end of the cylinder surface flush with the wall of the floor. Two protrusion models were tested, one being 1.5 mm in depth, and the other 3.0 mm in depth, Figure 7.

Each of the protrusions was tested in the Mach 4 facility with the apex of the model pointing upstream Figure 8 (a) and Figure (b). The result of using BCN165 liquid crystal as a shear stress indicator is clearly evident in Figure 8 where the shear stress distribution close to the protuberances for the two geometrical heights is observed.

An initial qualitative appraisal of the shear stress distribution shows that in the case of the wedge pointing upstream, Figure 8 (a) and Figure (b), the bow shock appears to be of the same distribution whereas the wakes are completely different, with the wake of the 3.0 mm wedge, Figure 8(b), showing a stronger bifurcated pattern than that of the 1.5 mm wedge, Figure 8 (a).

To fully understand the difference in these distributions, the value of the shear stresses within the bow shocks and the wakes are needed, and only a full-field analysis, rather than a point measurement system, will allow this realization.

1.5 mm high triangular wedge

3.0 mm high triangular wedge

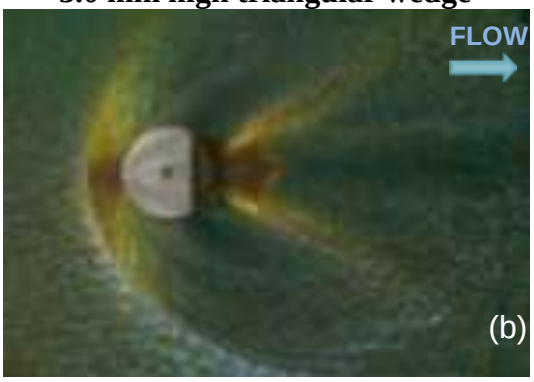

Fig. 8: Liquid Crystal Shear Stress Images showing Bow Shock and Wake distributions from 1.5mm and 3.0 mm wedge-shaped protuberances at Mach 4

A more detailed analysis, using software developed by ESI, has quantified this distribution by using the calibration curve for BCN165 shown in Figure 3. This software allows for an examination of the Hue at any location on the image and, in this case, provides the Hue value at discrete 1mm x 1mm areas along a predetermined line of finite length. The shear stress is then calculated from the Hue value using the calibration curve and the distribution along a line is determined. Figure 9 is a diagram of the locations that have been analyzed with this software at 4 upstream and downstream positions, and 2 locations on either side of the wedge models.

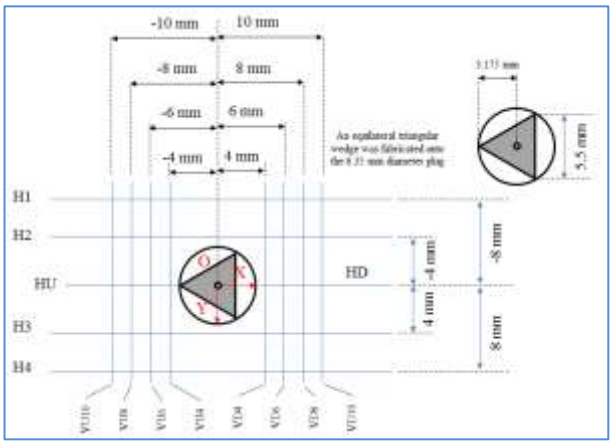

Fig. 9: Locations of the Shear Stress Profiles

4.1 1.5 mm High Wedge Pointing Upstream

Figure 10 provides the shear stress along 4 locations within the bow shock, at x = -4, -6, -8, and -10 mm from the center of the triangular wedge (center of the circular plug), and the wake region at x = 4, 6, 8, and 10 mm.

It may be observed in Figure 10[A] that the shear stress at the extremities of the locations is close to a value of about 130 ± 10 Pa, a value a little above the empty test section of 110 Pa as given by the distribution in Figure 6, and is probably the result of the introduction of the model. This value of approximately 130 Pa is relatively constant along the entire location at x = - 10mm indicating that the linear region is outside of the bow shock region; whereas at x = -8mm, there is a small reduction in the shear stress to about 70 Pa indicating that the exploratory line is now within the bow shock. As this exploratory line becomes closer to the wedge at x = -6 and -4 mm, the shear stress falls close to zero and is distributed ±12mm on either side of the center line of the wedge.

Within the wake region, Figure 10[B], close to the base of the wedge, at x = 4 and 6 mm, the shear stress is approximately zero over about 6 mm and

rises rapidly towards a value of about 200 Pa at a 'y' location of ± 7mm from the center line of the wedge, from whence it falls to the shear stress value for the tunnel of 130 ± 10 Pa. Further downstream at x = 8 and 10 mm, there is a large increase in the shear stress to about 240 Pa and 300 Pa respectively, and shows some asymmetry in these particular results, which can also be observed in Figure 8(a).

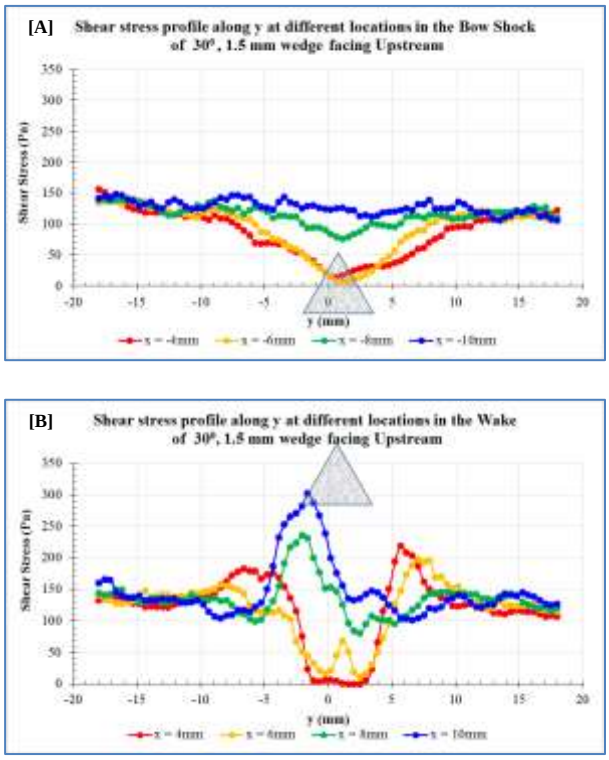

Fig. 10: Shear stress in the Bow Shock and Wake region of 1.5 mm high wedge facing upstream

4.2 3.0 mm High Wedge Pointing Upstream

The presence of this larger wedge geometry has a profound effect on the shear stress distribution as shown in the results of Figure 11. As with the 1.5 mm wedge, the distribution of the shear stress at the x = -8 and -10 mm lines are outside of the bow shock whereas the lines at x = -6 and -4 mm are within, Figure 11[A]. The image in Figure 8(b) shows that the bow shock is not completely symmetrical about the x-axis with the LC depicting a change in hue in the flow as the boundary layer approaches the shock. This change results in some higher values in shear stress between 200 – 250 Pa for the x = -8 and -10mm lines on the port side of the wedge, some 12 mm from the center line, reducing in value across the test section, to the tunnel value of 130 ± 10 Pa on the starboard side. The results for x = - 6mm case show that the shear stress falls to zero on the center line and is affected by the bow shock between y = ± 10mm, with the x = -4mm case providing similar results except on the starboard side where an abrupt change at the edge of the bow shock has taken place at y = 7mm.

The shear stress in the wake of this wedge geometry is most striking in that there appears to be a bifurcation of the wake, created by the sharp trailing edges of the wedge, Figure 8(b). The distribution of the shear stress at the locations of x = 4, 6, and 8 mm downstream of the rearward face of the wedge shows how the twin 'tails' of the wake are evolving. For the x = 4 mm case, the shear stress between y = ± 2mm is close to zero and rises to a peak of about 300+ Pa at y = ± 5mm and eventually falls to a value of about 200 ±20 Pa at y = ± 13mm. This is repeated for the x = 6mm case except that the distribution is wider with the peak rising to about 300 Pa at y = ± 7mm. These two distributions highlight the strength of the two bifurcation wakes close to the trailing edge of the wedge. At x = 8 mm, the distribution starts to indicate the change in the shear stress and provides for two distinct low shear stress regions at about y = ±4 mm, increasing the width of the wake and reaching a maximum of about 200 Pa. Further analysis of the x = 10 mm case demonstrates the evolving 'tails' of low shear stress at y = ±4 mm that allows a high shear stress of some 250 Pa to occur on the center line of the wedge.

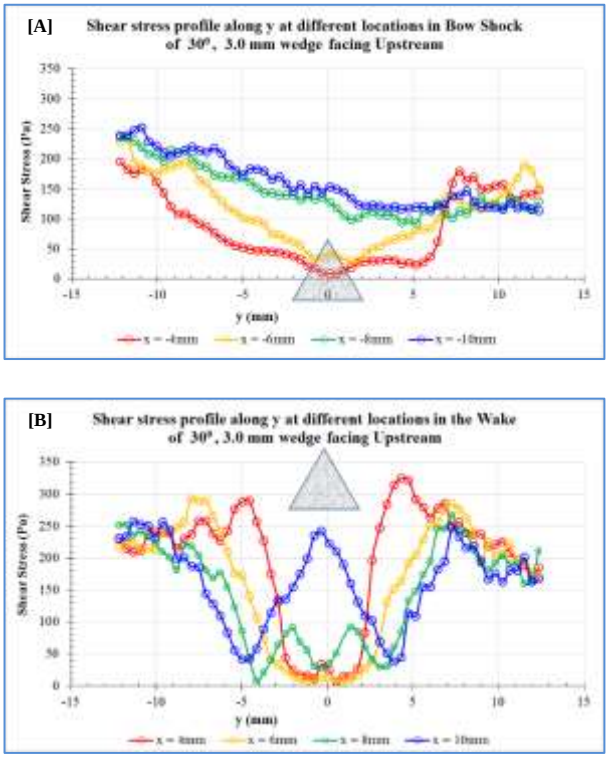

Fig. 11: Shear stress in the Bow Shock and Wake region of 3.0 mm high wedge facing upstream

The shear stress distribution in the streamwise x direction at two distinct positions of y = ±4 and ±8 mm for the 1.5 mm wedge is shown in Figure 12[A] and Figure [B]. The effect of the bow shock is clearly observable for the y = ±4 mm case where a surface shear stress of 130 Pa occurs before the bow shock from x = -20mm to about x = -10mm occurs, Figure 12[A]. The shear stress then decreases in magnitude through the bow shock, reaching a minimum at approximately x = -5mm from the wedge center, before increasing 6-fold through the wake of the bow shock, between 230 – 280 Pa, visibly observable in Figure 8. The shear stress again reduces to another minimum at approximately x = +5mm due to the wake structure before increasing a second time and returning to a more steady value of about 160 Pa. It is expected that this value of 160 Pa will persist some distance downstream before returning to the unobtrusive value of 130 Pa.

The shear stress further from the sides of the wedge at y = ±8mm shows a distribution similar to the y = ±4mm case but of much lower magnitude, Figure 12[B]. Although the overall effect on the distribution is lower, the effect of the bow shock and wake has increased the full field values upstream and downstream of the wedge to about 140 Pa.

1.5 mm high wedge facing UPSTREAM

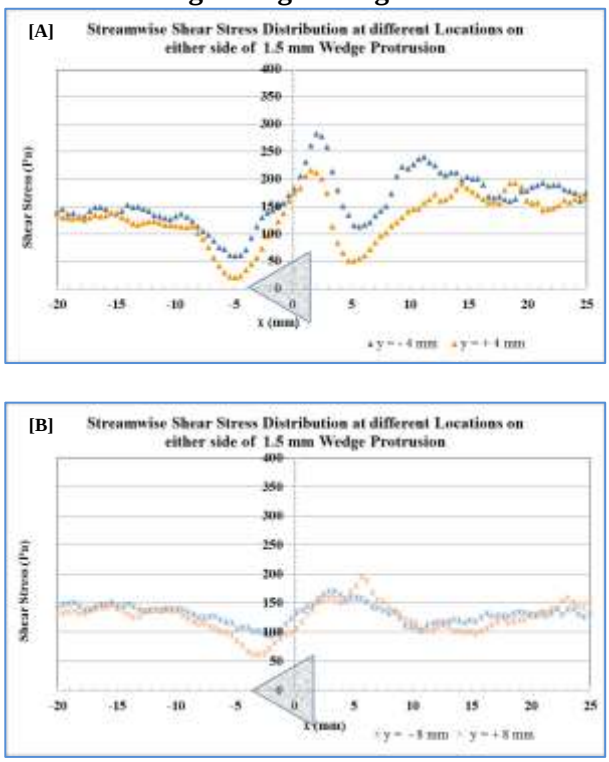

Fig. 12: Shear stress on either side of the 1.5 mm high wedge facing upstream

The shear stress distributions caused by the bow shock and the wake from the 3.0mm high wedge are similar in structure to that of the 1.5 mm wedge but of much greater magnitude, Figure 13[A] and Figure [B]. In the case of the distribution for y = ±4mm, much stronger shear stress occurs behind the bow shock between 280 and 350 Pa (the difference in these values may be due to a small misalignment of the 'y' data lines on either side of the model). It may also be noted that the minimum value in the shear stress is lower in the wake region compared to the 1.5 mm high wedge, and the downstream full field value, at x = +25mm, is much higher at approximately 250 Pa. The implications of these dramatic changes in the shear stress for such a small change in the height of a protuberance cannot be overstated.

At the location of y = ±8mm, the shear stress distribution is, again, similar to that for the 1.5mm wedge but of higher magnitudes, Figure 13[B]. Furthermore, the location of the minimum value of the shear stress caused by the bow shock and the wake have both receded downstream for the y =± 8mm case compared to that for the y = ±4mm case.

3.0 mm high wedge facing UPSTREAM

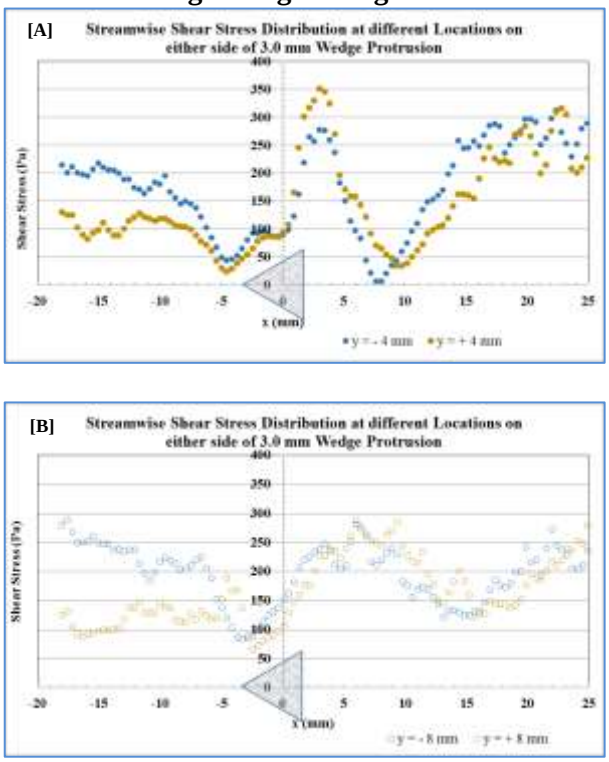

Fig. 13: Shear stress on either side of the 3.0 mm high wedge facing upstream

5 Conclusions

A mechanical calibration rig has been used successfully to calibrate a liquid crystal, BCN165, supplied by SpotSee. The design and fabrication of the calibration rig were supplied by Engineering & Scientific Innovations Inc, along with software for the calibration and measurement routines. Measurements of the shear stress distribution caused by a small equilateral wedge-shaped protuberance in a Mach 4 flow have been achieved. Two sizes of wedges were used, one being 1.5mm high with a base of 5.5mm, the other 3.0mm high with a base of 5.5mm, and an area of 13.1 mm^2. An analysis of the shear stress through the bow shock and wake formations has shown:-

a) A small protuberance of 13.1 mm^2 can affect the surface flow field significantly
b) The presence of these small protuberances increases the empty test section full field shear stress
c) The shear stress distribution through the bow shock of the protuberance may be mapped
d) The shear stress through the wake region of the protuberance highlights the wake structure
e) The shear stress downstream of the protuberances indicates, as expected, a strong wake region.

Further studies are needed to quantify the effect of the height of protuberances in relation to the boundary layer thickness in high Mach number flows.

The ability of Liquid Crystals to measure shear stress has been explored over many years but the use of them has been mainly for research purposes whereby the technique has been the subject of the study. This work highlights the ability to use calibrated Liquid Crystals to measure the shear stress generated by small 3-D protrusions, which are very prevalent on high-speed platforms, including those that are supersonic and hypersonic in form. Without a doubt, hypersonic platforms are being designed and constructed and the CFD/simulation community responsible for their designs would benefit from a better understanding of the shear stress generated around 3-D protuberances. The present work has highlighted the extent that a small protuberance has on the local shear stress and although this has been measured in a Mach 4 flow, it is expected that a similar result would occur at lower and higher Mach numbers.

Acknowledgement:
The authors would like to thank Dr. Eric Marineau for his intuitive understanding of the problems of measuring surface shear stress at high Mach numbers and his many helpful suggestions that have enabled this work to proceed.

References:

[1] Ash J I, "Liquid Crystals for Nondestructive Evaluation". No. Ntiac-78-2. *Nondestructive Testing Information Analysis Center* San Antonio Tx, 1978, [Online]. https://apps.dtic.mil/sti/tr/pdf/ADA129084.pdf (Accessed Date: December 23, 2024).

[2] Roberts G T & EastR A, "Liquid crystal thermography for heat transfer measurement in hypersonic flows-A review." *Journal of spacecraft and rockets* 33.6: 761-768. 1996. doi: 10.2514/3.26835

[3] Reda, D.C., Wilder M C, & Farina, D J, "New methodology for the measurement of surface shear stress vector distribution". *AIAA J*, 35 (4) 608-614, 1997. doi: 10.2514/2.165

[4] Reda D C, Wilder M C & Mehta R D, "Measurement of continuous pressure and shear distributions using coating and imaging techniques". *AIAA J*, 36 (6) 895-899, 1998. doi: 10.2514/2.484

[5] Hay J L, & Hollingsworth D K. "A comparison of trichromic systems for use in the calibration of polymer-dispersed thermochromic liquid crystals." *Exp Therm Fluid Sci*, 12: 1–12, 1996. doi: 10.1016/0894-1777(95)00013-5.

[6] Syed Qasim Zaheer, Peter J. Disimile, and Norman Toy, "Assessment of Hue Transformation Algorithms for SSLC's Studies", *American Journal of Engineering Research, (AJER)*, Vol-10, Issue-8, pp 276-284, 2021, [Online]. https://www.ajer.org/papers/Vol-10-issue-8/ZE1008276284.pdf (Accessed Date: December 23, 2024).

[7] Klein E J & Margozzi A P, "Apparatus for the calibration of shear sensitive liquid crystals." *Review of Scientific Instruments* 41.2: 238-239, 1970. doi: 10.1063/1.1684477

[8] Parmar D S, "A novel technique for response function determination of shear sensitive cholesteric liquid crystals for boundary layer investigations." *Review of scientific instruments* 62.6: 1596-1608, 1991.doi: 10.1063/1.1142438.

[9] Zhao J, "Investigation on wall shear stress measurement in supersonic flows with shock waves using shear-sensitive liquid crystal coating." *Aerospace science and Technology* 85: 453-463, 2019. doi: 10.1016/j.ast.2018.12.034.

[10] Reda D C & Muratore Jr J J, "Measurement of surface shear stress vectors using liquid crystal coatings." *AIAA journal* 32.8: 1576-1582, 1994. doi: 10.2514/3.12146.

[11] Fujisawa N, Funatani S & Kosaka S, "Measurement of shear-stress distribution by liquid-crystal coating." *Optical Technology and Image Processing for Fluids and Solids Diagnostics, Beijing*, 2002. Vol. 5058. *International Society for Optics and Photonics*, 2003. doi: 10.1117/12.509840.

[12] Zhao J, Scholz P & Gu L X. "Measurement of surface shear stress vector distribution using shear-sensitive liquid crystal coatings." *Acta Mechanica Sinica* 28.5: 1261-1270, 2012. doi: 10.1007/s10409-012-0144-1.

[13] Wang C P, Zhao J, Jiao Y & Cheng K M, "Measurement of surface shear stress vector beneath high-speed jet flow using liquid crystal coating." *Modern Physics Letters B* 32.12n13: 1840029. 2018. doi: 10.1142/S0217984918400298.

[14] Fujisawa N., Aoyama A. & Kosaka S., "Measurement of shear-stress distribution over a surface by liquid-crystal coating." *Measurement Science and Technology* 14.9: 1655, 2003. doi 10.1088/0957-0233/14/9/317.

[15] Reda D C & Aeschliman D P, "Liquid crystal coatings for surface shear-stress visualization in hypersonic flows." *Journal of Spacecraft and Rockets* 29.2: 155-158, 1992. doi: 10.2514/3.26329.

Contribution of Individual Authors to the Creation of a Scientific Article (Ghostwriting Policy)

The authors equally contributed in the present research, at all stages from the formulation of the problem to the final findings and solution.

Sources of Funding for Research Presented in a Scientific Article or Scientific Article Itself

No funding was received for conducting this study.

Conflict of Interest

The authors have no conflicts of interest to declare.